ROYAL INSTITUTE OF TECHNOLOGY, SCHOOL OF INDUSTRIAL ENGINEERING AND MANAGEMENT

Analysis and Design of an Electric Nut Runner for Tightening of Bolted Joints

Alexandra Tang, Daniela Attalla, Pallav Rawat

October 31, 2016

CONTENTS

1. Introduction **3**

2. DC Motor Model **3**
2.1. Verification 5
2.2. PD-Controller 7
2.3. Model Simplification 8
2.4. Gear Ratio 9

3. Complete Nut-Runner Model **10**
3.1. Intertias 10
3.2. State Space Model 11
3.3. PI-Controller 13

4. Bolt Tightening Model **14**
4.1. PI controller 16
4.2. Tensile Stress 19
4.2.1. Extended Model with Coulomb Friction 20

5. Operator Model **21**
5.1. Energy Consumed 24

Appendices

A. Data Sheet of DC-motor **26**

B. Thorough Derivation of Diameter **27**

1. Introduction

Hand held electric nut runners are used in the manufacturing industry to aid assembly workers in doing precisely controlled bolt tightening, e.g. in the automotive industry. Such a nut runner is a good example of a quite advanced mechatronic system for which the characteristics of the device itself, of the bolted assembly and of the human operator must be considered and analysed together during the design process. In this report an electric nut-runner will be modelled and analyzed.

2. DC Motor Model

The electrical part of a voltage driven DC-motor can be seen in Figure 2.1. This gives the following equation

$$u = L\frac{di}{dt} + Ri + K_{emf}\dot{\varphi}, \tag{2.1}$$

where u is the applied voltage, L is the inductance of the motor, R is the resistance, i is the current, K_m is the back electromotive force and $\dot{\varphi}$ the speed of the rotor.

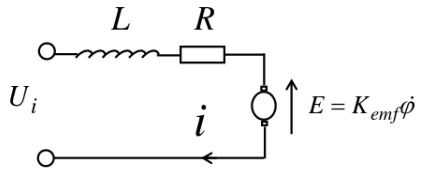

Figure 2.1: Electrical part of a DC-motor.

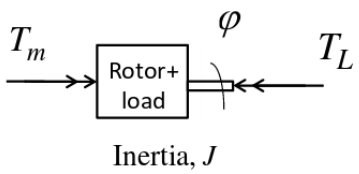

Figure 2.2: Mechanical part of a DC-motor.

The generated torque in the output shaft of the motor is

$$J\ddot{\varphi} = T_m - T_L, \tag{2.2}$$

as concluded from Figure 2.2. However, since there is no external torque in the modelling of the DC-motor only, the equation can be simplified to

$$J\ddot{\varphi} = T_m = K_m i, \tag{2.3}$$

where J is the inertia of the output shaft, T_m is the motor torque, $\ddot{\varphi}$ is the angular acceleration and K_m is the motor torque constant.

Equation 2.1 and Equation 2.3 were used to build a block diagram of the DC-motor model, which is shown in Figure 2.3 below.

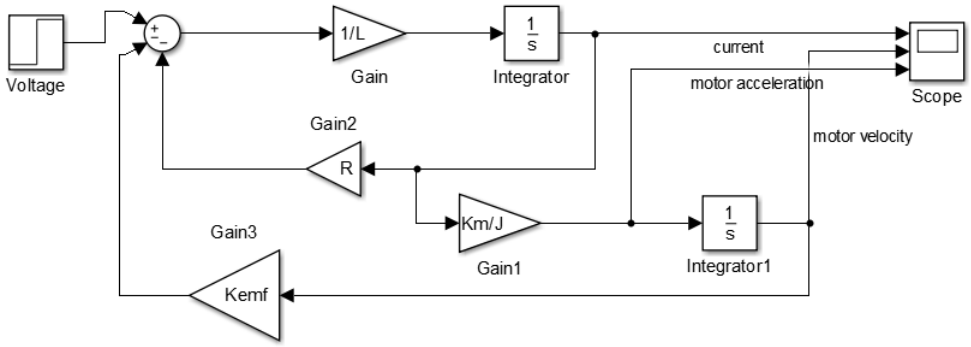

Figure 2.3: Block diagram of the DC-motor model.

The current and the angular velocity were chosen to be the states in the state space model that was to be modelled

$$\begin{cases} x_1 = i \\ x_2 = \dot{\varphi} \end{cases} \tag{2.4}$$

From Equation 2.1 and 2.3 the state variables could be derived to the following

$$\dot{x_1} = \frac{di}{dt} = \frac{u - Ri - K_{emf}\dot{\varphi}}{L}, \tag{2.5}$$

$$\dot{x_2} = \ddot{\varphi} = \frac{T_m}{J} = \frac{K_m i}{J} \tag{2.6}$$

With this, the state space model became

$$\begin{bmatrix} \dot{x_1} \\ \dot{x_2} \end{bmatrix} = \begin{bmatrix} \frac{-R}{L} & \frac{-K_{emf}}{L} \\ \frac{K_m}{J} & 0 \end{bmatrix} \begin{bmatrix} x_1 \\ x_2 \end{bmatrix} + \begin{bmatrix} \frac{1}{L} \\ 0 \end{bmatrix} u \tag{2.7}$$

The DC-motor was also modelled using a transfer function. It was derived by using the differential equations, Equation 2.1 and Equation 2.3, as shown below.

$$\begin{aligned} U(s) &= LsI(s) + RI(s) + k_{emf}\omega(s) \\ Js\omega(s) &= k_m I(s) \\ U(s) &= \frac{LJs^2}{k_m}\omega(s) + \frac{RJs}{k_m}\omega(s) + k_{emf}\omega(s) \\ G(s) &= \frac{\omega(s)}{U(s)} = \frac{1}{\frac{LJ}{k_m}s^2 + \frac{RJ}{k_m}s + k_{emf}} \end{aligned} \tag{2.8}$$

2.1. VERIFICATION

A voltage step of 24V was applied on the input to verify that the DC-motor model was working correctly. The voltage value was chosen according to the motor specifications (Appendix A). The time-domain response in terms of current, angular velocity and angular acceleration is illustrated in Figure 2.5. The step response is shown in Figure 2.4. The DC motor-model was then compared to the data sheet by using the values found in the figures just mentioned. This comparison is seen in Table 2.1 below.

Table 2.1: Comparison of the data sheet and the DC-motor model

	Stall torque	No-load speed	Angular acceleration	Mechanical time constant
Data sheet	718 mNm	5500 rpm	$120 \cdot 10^3$ rad/s^2	4.6 ms
DC-motor model	682 mNm	5269 rpm	$114 \cdot 10^3$ rad/s^2	4.57 ms

The table above clearly shows that the DC-motor model is performing accurately and according to the preferences.

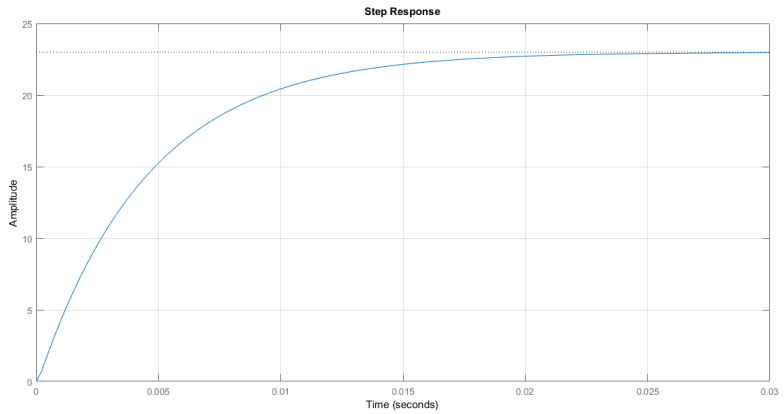

Figure 2.4: Step Response

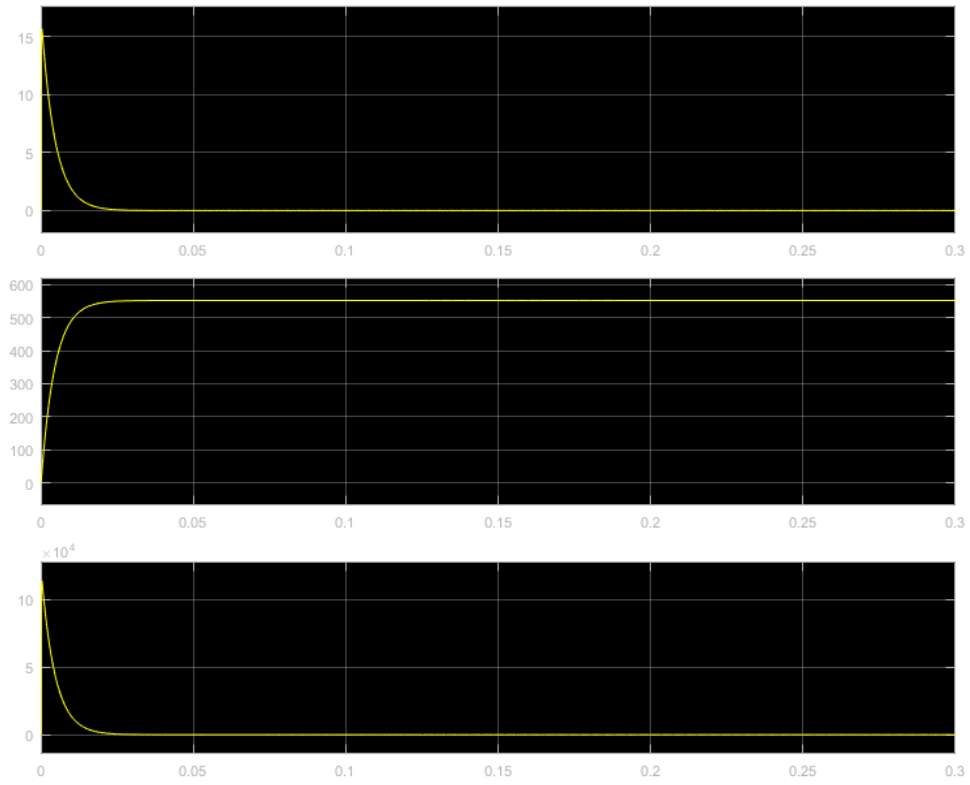

Figure 2.5: Current (top), angular velocity (middle) and angular acceleration (bottom) in time-domain.

2.2. PD-CONTROLLER

An angular velocity controller for the DC-motor was developed and implemented as

$$u_c = k_p(\omega_{ref} - \omega) - k_d\dot{\omega}, \tag{2.9}$$

where k_p and k_d were the proportional and derivative control gains respectively. The controller was tuned to make a quick response without overshooting or violating any voltage or current limitations of the motor, to an input reference step of 12 rad/s. The k_p value was chosen as 2 and the k_d value was chosen according to

$$k_d = \frac{c_v n_o}{5}, \tag{2.10}$$

where c_v is the dynamic friction torque and n_o the no-load speed of the motor. This was to achieve the same damping factor as given by the motor resistance. Hence, k_d was chosen as 0.0014. The block diagram model of the system is demonstrated in Figure 2.6.

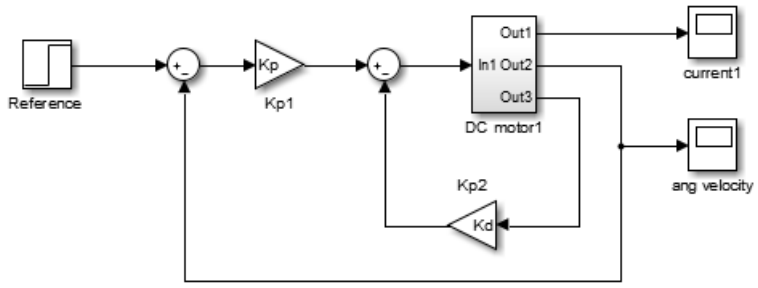

Figure 2.6: Block diagram of DC-motor model with PD control.

As seen in Figure 2.7 the angular velocity is close to the reference step of 12 rad/s.

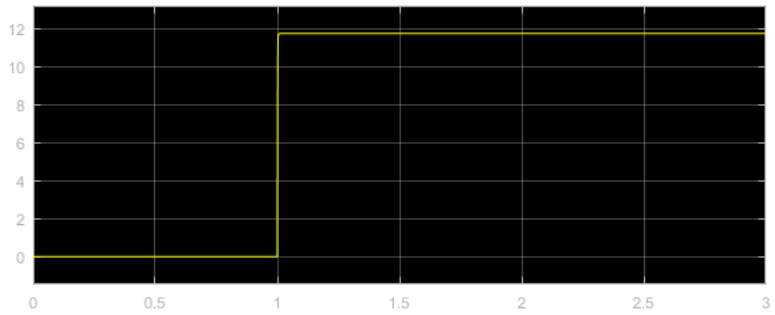

Figure 2.7: Angular velocity of motor with PD control.

2.3. Model Simplification

The rotor inductance in DC-motors is usually very low and can be disregarded. To confirm this, the location of the poles in the simplified model without the inductance was compared with the original one.

The modelled system were inductance was included gave two poles, one at p_1= -13000 and one at p_2=-221 as seen in Figure 2.8.

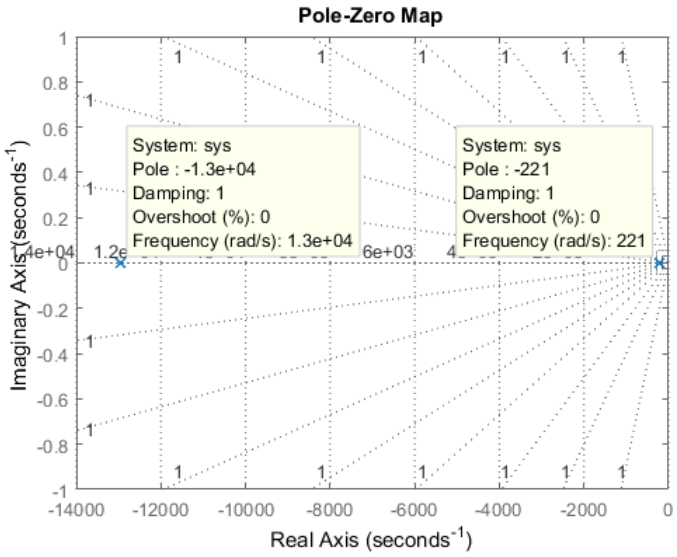

Figure 2.8: Pole location of the motor without control.

The pole closest to the imaginary axis on the s-plane, i.e. p_2, was the one dominating the response of the system since it was the slowest one and gave a mechanical time constant of 0.00457 ms as mentioned in Table 2.1.

The model in which the rotor inductance was neglected had the following differential equation

$$\ddot{\varphi_1} = \frac{K_m i}{J} = \frac{K_m}{R}(U - K_{emf}\dot{\varphi_1}), \tag{2.11}$$

with the resulting block diagram as shown in Figure 2.9.

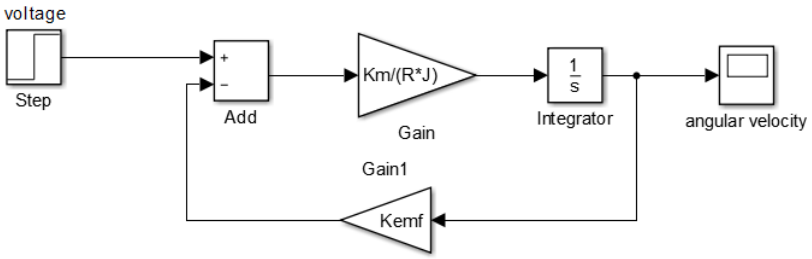

Figure 2.9: Block diagram of the simplified motor model.

The new simplified model generated one pole as depicted in Figure 2.10.

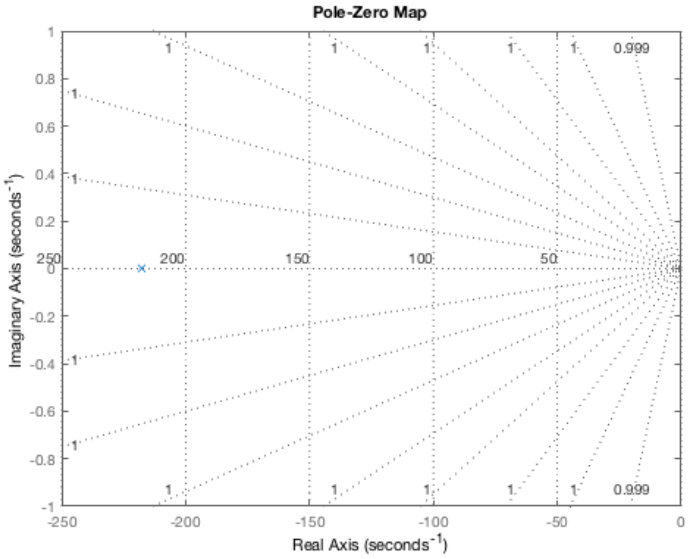

Figure 2.10: Pole location of the motor were the rotor inductance is neglected.

This pole is the same dominant one as in the previous model where the rotor inductance was included and the system can therefore be simplified as described.

2.4. Gear Ratio

The tool consists of two planetary gears with equal gear ratios. An electrical motor is typically associated with two torque specifications; stall-torque and continuous torque. However, since the nut-runner does not operate continuously, only stall-torque will be taken into account when deciding the gear ratio.

The total gear ratio is calculated according to

$$N = \frac{T_{out}}{T_s}, \tag{2.12}$$

where T_{out} is the maximum torque on the nut-runner and T_s is the stall-torque. With numerical values the total gear ratio is 69.64. Hence, the gear ratio for each gear is 8.34.

3. Complete Nut-Runner Model

A model of the complete tool and nut rotation for the rundown phase was derived using the previously developed simplified motor model. An idealized transmission model of this can be seen in Figure 3.1.

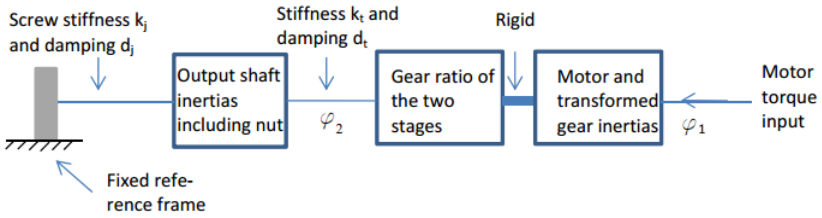

Figure 3.1: Idealized transmission model.

3.1. Intertias

For the combined inertias the below notations were used

$$J_{mg} = J_{motor,rotor} + J_{gears}, \tag{3.1}$$

$$J_{out} = J_{outputshaft} + J_{nut}. \tag{3.2}$$

The inertia of a planetary gear stage can be estimated according to

$$J_g = \frac{\rho_g \pi r_g^4 (9bn^2 - 36bn + 52b)}{32 C_{gr}^4 (n-1)^4} \tag{3.3}$$

where $C_{gr} = \frac{r_g}{r_{gr}}$, ρ_g is the material density and n is the gear ratio for a single gear. There are two planetary gear stages in the gear box of the tool and the numerical values for both of them are declared in Table 3.1.

Table 3.1: Parameters used in the calculations of the gear intertias.

	Gear 1	Gear 2
r_g	0.0185	0.0185
r_{gr}	0.0163	0.0163
b	0.006	0.006
b_c	0.013	0.0049

With Equations 3.1 and 3.2, the equilibrium equations considering the torques can be put as shown in Figure 3.2.

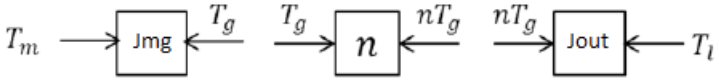

Figure 3.2: Equilibrium on the nut-runner model

If the modelling starts from the motor end, the torque gets multiplied and the angular velocity gets divided by the corresponding gear ratio. From here the below differential equations from constitutive modelling of the inertias' angular acceleration were derived as

$$\begin{aligned} J_{mg}\ddot{\varphi}_1 &= T_m - \frac{1}{n^2}T_L \\ &= \frac{k_m}{R}u - \frac{k_m k_{emf}}{R}\dot{\varphi}_1 - \frac{k_t}{n^2}\left(\frac{\varphi_1}{n^2} - \varphi_2\right) - \frac{d_t}{n^2}\left(\frac{\dot{\varphi}_1}{n^2} - \dot{\varphi}_2\right) \end{aligned} \tag{3.4}$$

$$\begin{aligned} J_{out}\ddot{\varphi}_2 &= T_{L\varphi} - T_j \\ &= k_t\left(\frac{\varphi_1}{n^2} - \varphi_2\right) + d_t\left(\frac{\dot{\varphi}_1}{n^2} - \dot{\varphi}_2\right) - d_j\dot{\varphi}_2 \end{aligned} \tag{3.5}$$

3.2. State Space Model

A state space model on the form

$$\begin{aligned} \dot{x} &= Ax + Bu \\ y &= Cx + Du \end{aligned} \tag{3.6}$$

was derived using the following state vector

$$\begin{bmatrix} x_1 \\ x_2 \\ x_3 \\ x_4 \end{bmatrix} = \begin{bmatrix} \varphi_1 \\ \varphi_2 \\ \dot{\varphi}_3 \\ \dot{\varphi}_4 \end{bmatrix}, \tag{3.7}$$

where φ_1 and φ_2 are the motor and nut angles respectively and $\dot{\varphi}_1$ and $\dot{\varphi}_2$ are the motor and nut angular velocities.

With the differential equations from Equation 3.4 and Equation 3.5, the matrices were formed as:

$$A = \begin{bmatrix} 0 & 0 & 1 & 0 \\ 0 & 0 & 0 & 1 \\ -\frac{k_t}{J_{mg}n^4} & \frac{k_t}{n^2 J_{mg}} & -\frac{\frac{K_m K_{emf}}{R}+\frac{d_t}{n^4}}{J_{mg}} & \frac{d_t}{J_{mg}n^2} \\ \frac{k_t}{J_{out}n^2} & -\frac{k_t}{J_{out}} & \frac{d_t}{J_{out}n^2} & -\frac{d_t+d_j}{J_{out}} \end{bmatrix}$$

$$B = \begin{bmatrix} 0 \\ 0 \\ \frac{k_m}{J_{mg}R} \\ 0 \end{bmatrix} \qquad C = \begin{bmatrix} 1 & 0 & 0 & 0 \\ 0 & 1 & 0 & 0 \\ 0 & 0 & 1 & 0 \\ 0 & 0 & 0 & 1 \end{bmatrix} \qquad D = \begin{bmatrix} 0 \\ 0 \\ 0 \\ 0 \end{bmatrix} \tag{3.8}$$

The state-space model is implemented in MATLAB by inputting the matrices A through D into the native ss() function. Likewise, the state-space model is implemented into Simulink by inputting A through D into the State-Space block. The step response of the system to an input voltage of 1 V can be seen in Figure 3.3.

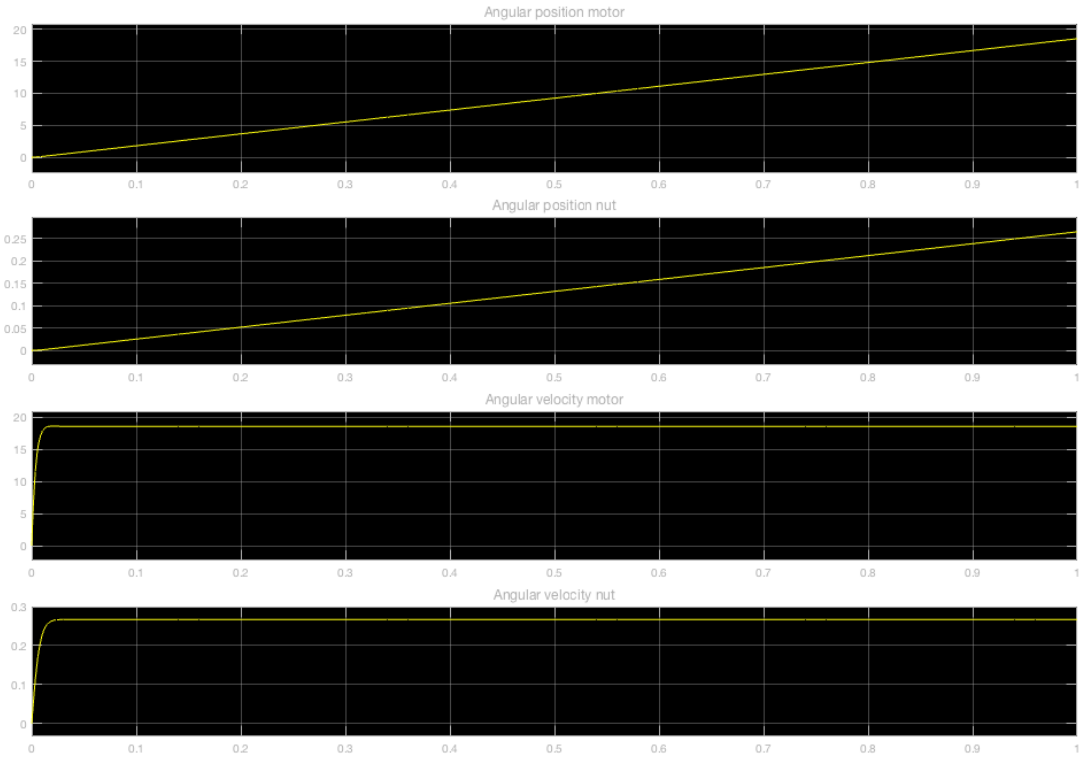

Figure 3.3: The step response of the system to an input voltage of 1 V.

As can be seen in Figure 3.3 scaling between the output parameters and the input parameters is approximately 70 which is close to the previously calculated total gear ratio, which proves the correctness of the developed model.

3.3. PI-Controller

A PI-controller was developed to control the angular velocity of the nut during the rundown phase. The control target was to follow a reference signal of 3 rad/s with smooth response and without overshoot or steady-state error. By manually tuning the control system parameters, the proportional gain k_p was set to 8.5 and the integral gain to k_i to 10. The response of the system can be seen in Figure 3.4 and it is clear that the system does not overshoot, nor exhibit steady state error.

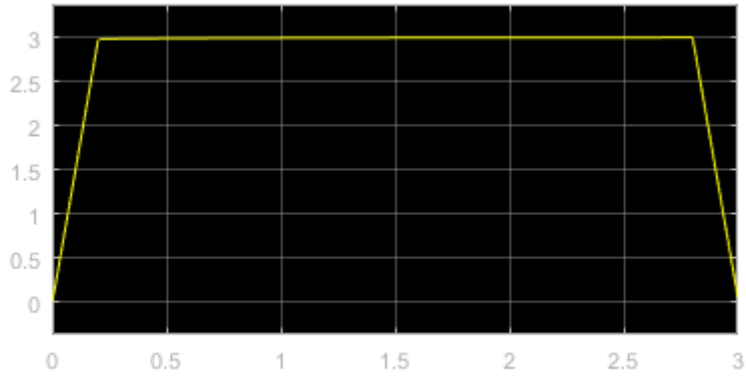

Figure 3.4: The angular velocity of the nut with k_p =8.5 and k_i = 10.

As seen in Figure 3.5, the voltage does not exceed any limits.

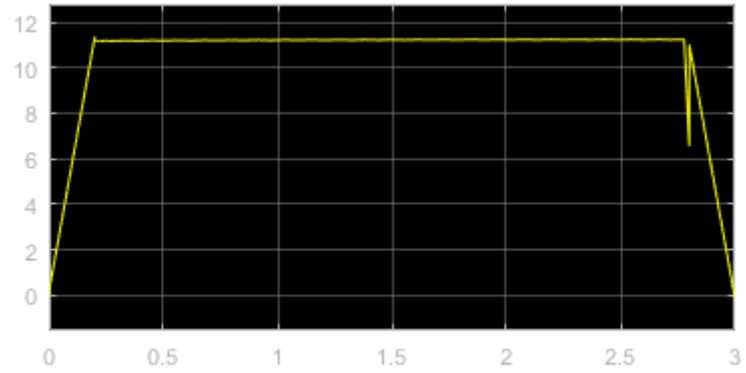

Figure 3.5: The input voltage with the implemented PI-controller.

4. Bolt Tightening Model

The complete nut-runner model from the previous section was extended to include the screw-nut-joint subsystem in order to make a model that corresponds to Figure 3.1. The run-down and alignment phases were assumed to have passed in the bolt tightening process. Another assumption was that the elastic clamping phase starts at zero velocity. A M8 screw of strength class 8.8 with a pitch of 1.25 mm and a free length of 100 mm was used.

The translational stiffness of the screw, k_j, was calculated using the formula

$$k_j = \frac{A_s E}{L} \tag{4.1}$$

where E is the Young's modulus of steel, L is the length of the screw and A_s is the nominal cross-sectional area of the screw. The cross-sectional area was calculated using the following diameter

$$d_s = D - \frac{13}{12} H \tag{4.2}$$

where D is the nominal screw diameter and H is

$$H = \frac{\sqrt{3}}{2} p \tag{4.3}$$

The pitch of the screw is here denoted as p. A more thorough derivation is presented in Appendix B. The values of the parameters in the Equation 4.1-4.3 are given in Table 4.1

Table 4.1: Parameters used in the bolt tightening model.

E	L	D	p
200 GPa	100 mm	8 mm	1.25 mm

The translational stiffness was then translated into rotational stiffness, k_r, acting on the nut. This was done by calculating the potential energy of the screw and the nut respectively and then making them equal to each other. This eventually resulted in

$$k_r = k_j \left(\frac{p}{2\pi} \right)^2 \tag{4.4}$$

The rotational stiffness was then used to update the nut-runner state space model to a bolt tightening state space model, which is presented below.

$$A = \begin{bmatrix} 0 & 0 & 1 & 0 \\ 0 & 0 & 0 & 1 \\ -\frac{k_t}{n^4 J_{mg}} & \frac{k_t}{n^2 J_{mg}} & -\left(\frac{k_m k_{emf}}{R J_{mg}} + \frac{d_t}{n^4 J_{mg}} \right) & \frac{d_t}{n^2 J_{mg}} \\ \frac{k_t}{n^2 J_{out}} & -\frac{k_t + k_r}{J_{out}} & \frac{d_t}{n^2 J_{out}} & -\frac{d_t + d_j}{J_{out}} \end{bmatrix} \tag{4.5}$$

$$B = \begin{bmatrix} 0 \\ 0 \\ \frac{k_m}{J_{mg} R} \\ 0 \end{bmatrix} \quad C = \begin{bmatrix} 1 & 0 & 0 & 0 \\ 0 & 1 & 0 & 0 \\ 0 & 0 & 1 & 0 \\ 0 & 0 & 0 & 1 \end{bmatrix} \quad D = \begin{bmatrix} 0 \\ 0 \\ 0 \\ 0 \end{bmatrix}$$

The torque on the nut and the corresponding turning angle for a 24V input voltage to the motor is presented in Figure 4.1 and Figure 4.2 respectively. The first figure clearly shows that

the torque does not exceed 50 Nm which is plausible as it is the maximum torque from the nut-runner. The corresponding turning angle reaches a value of 17.3 rad.

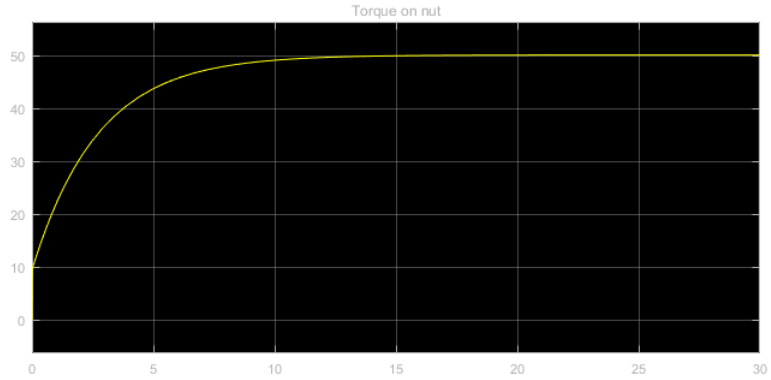

Figure 4.1: The torque on the nut given a 24V input voltage

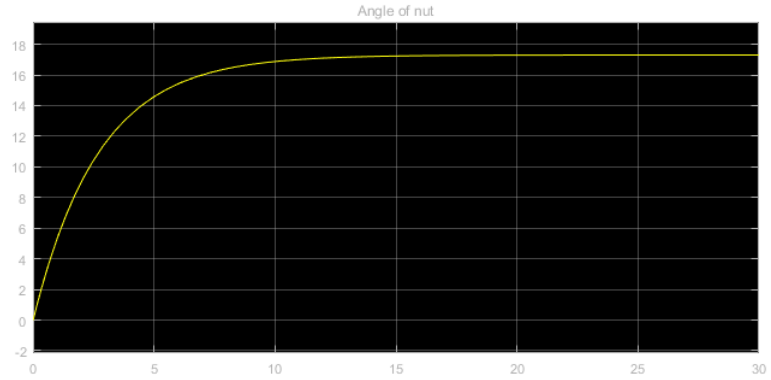

Figure 4.2: The turning angle of the nut given a 24V input voltage

4.1. PI CONTROLLER

The angular velocity controller for the elastic clamping phase was developed while considering the tool to be fixed. The elastic clamping phase was assumed to start at zero velocity and end when the targeted tightening torque of 25 Nm was reached. This was possible by using a torque limiter that switched off the system at 25 Nm. The run-down and alignment phases were assumed to have passed in the bolt tightening process and the targeted tightening speed was 3 rad/s. Two different controllers were implemented, a P-controller and a PI-controller according to Figure 4.3.

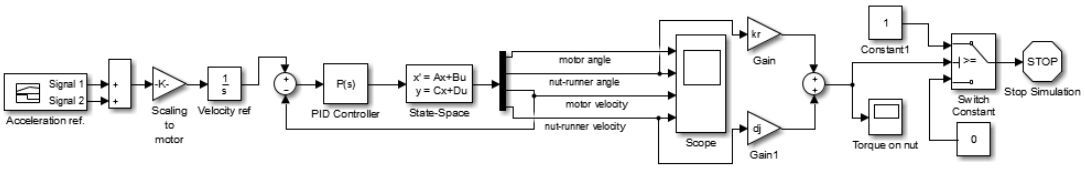

Figure 4.3: Block diagram of the system.

The system response with P-control is presented in Figure 4.4, where the proportional control gain k_p was set to 8.5.

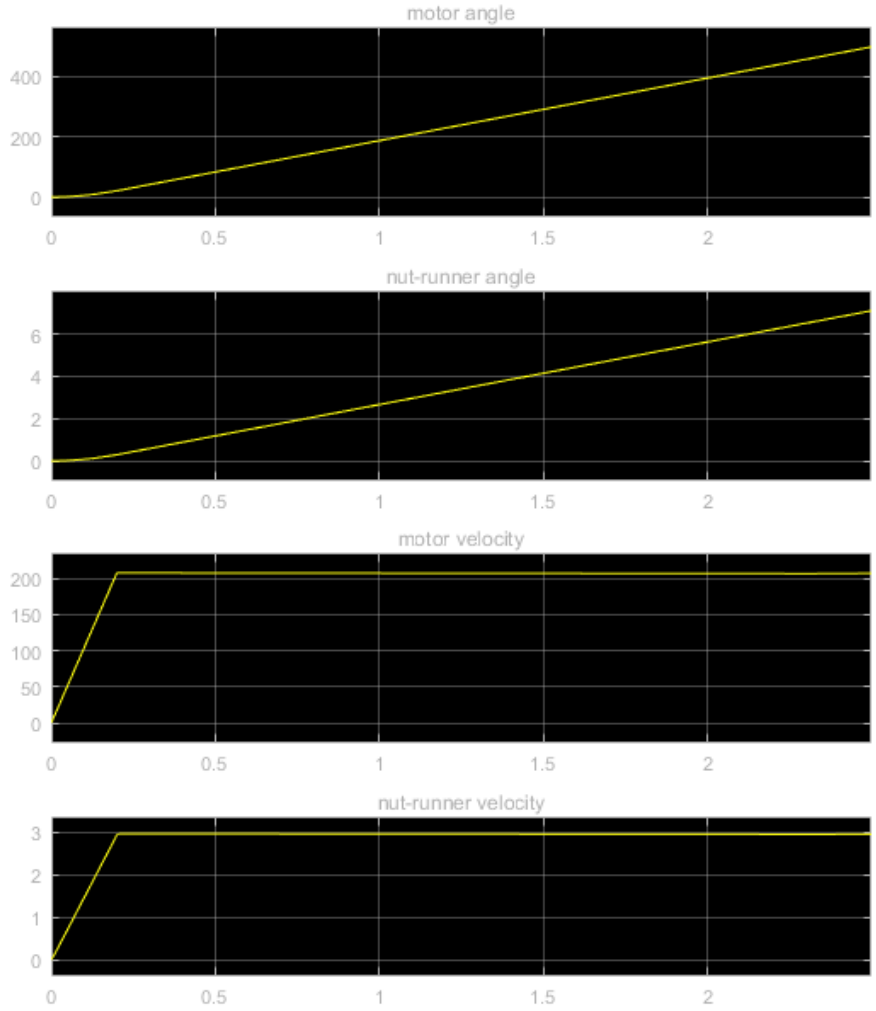

Figure 4.4: System response with P-control.

The system response with PI-control is presented in Figure 4.5, where the proportional and the integral control gain were set to $k_p = 8.5$ and $k_i = 10$. The velocity is following the reference signal and the tightening torque does not exceed the target torque of 25 Nm as seen in Figure 4.6.

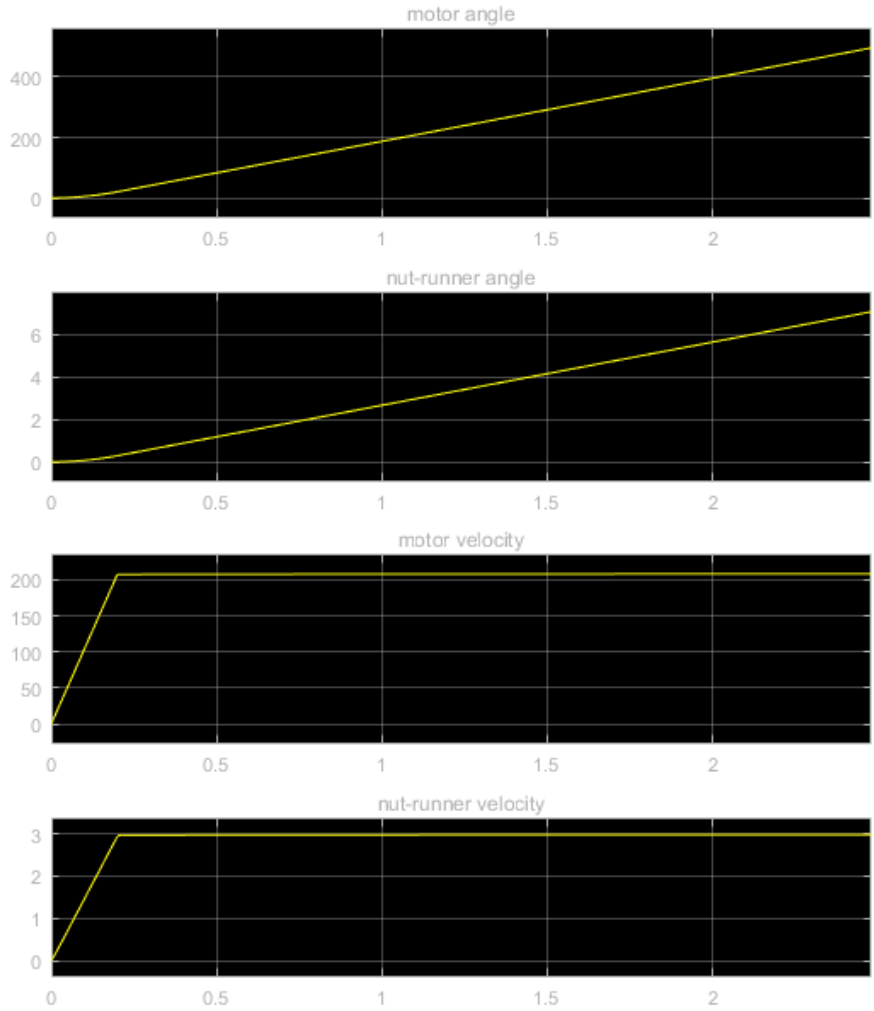

Figure 4.5: System response with PI-control.

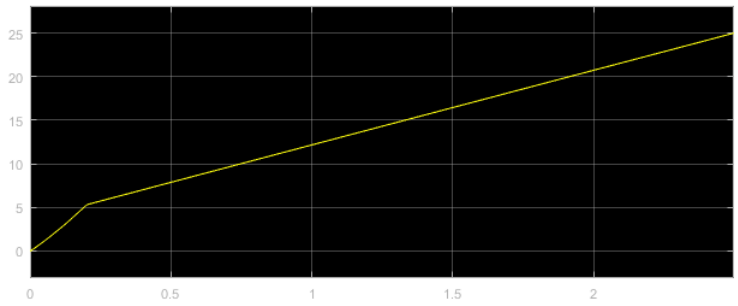

Figure 4.6: Tightening torque.

4.2. Tensile Stress

The bolt and nut that were to be tightened corresponded to a M8 screw of class 8.8. The yield strength of such a screw, i.e. the point at which plastic deformation occurs, was calculated as $800 \cdot 0.80 = 640$ MPa.

The screw was seen as acting as a spring, thus the tensile stress on the screw was calculated according to the formula below

$$\sigma = \frac{F_s}{A_s} = \frac{kx}{A_s} = \frac{k_j(\varphi_2)\frac{p}{2\pi}}{\frac{\pi d^2}{4}}. \tag{4.6}$$

While comparing the tensile stress curve with the yield strength with regards to the tightening nut angle, as seen in Figure 4.7, it could be concluded that the force acting on the screw was too high since the tensile stress curve exceeded the yield strength. The tightening angle was measured to be 7 rad.

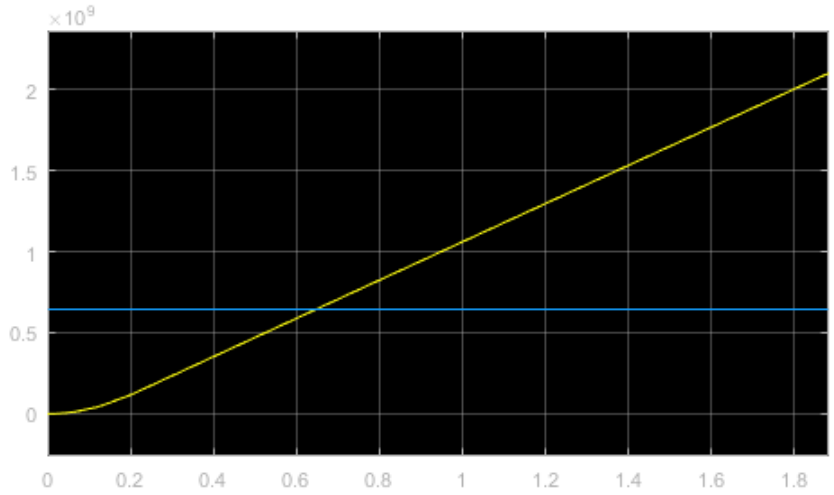

Figure 4.7: Tensile stress (yellow curve) during bolt tightening compared to the yield strength (blue curve) of the screw material.

4.2.1. Extended Model with Coulomb Friction

Since the force on the screw was too high, the model was extended with coloumb friction torque between nut and screw according to

$$T_{friction} = \mu F_s r_s, \tag{4.7}$$

where μ was the friction coefficient set as 0.2, F_s was the force on the screw and r_s was the nominal radius on the thread. By adding friction torque, the total torque on the nut reaches the target torque faster, preventing the tensile stress on the screw to exceed the yield strength. The tensile stress of the new model was plotted and compared with the yield strength in Figure 4.8.

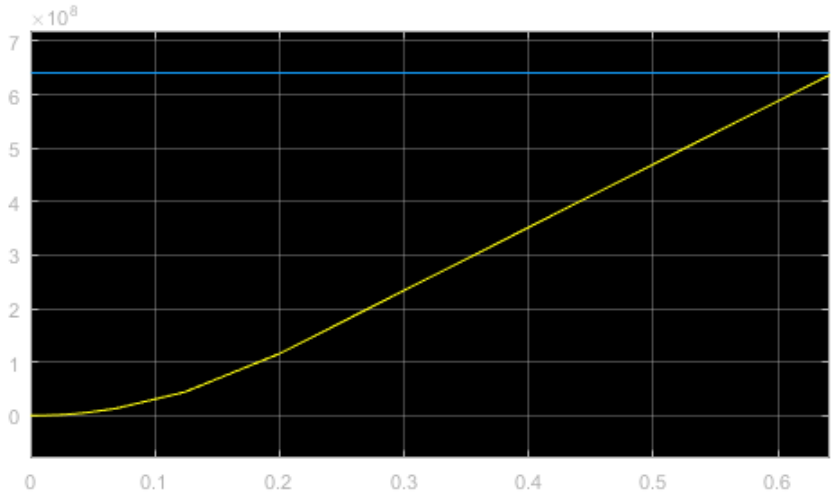

Figure 4.8: Tensile stress (yellow curve) with Coloumb friction during bolt tightening compared to the yield strength (blue curve) of the screw material.

As can be seen, the achieved tightening is now below the yield strength, but at the same time close to it. It is therefore in good order, with a tightening angle of 1.60 rad and the deflection angle 0.0121 rad.

5. Operator Model

The bolt tightening model with Coulomb friction was further extended by adding the operator model shown in Figure 5.1.

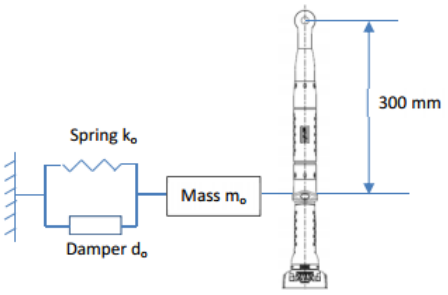

Figure 5.1: Operator model.

Since the tool was no longer fixed, the angular motion of the nut was not equivalent to the angular motion of the output shaft. This change made the system go from a fourth order model to a sixth order model with the state vector defined as

$$\begin{bmatrix} x_1 \\ x_2 \\ x_3 \\ x_4 \\ x_5 \\ x_6 \end{bmatrix} = \begin{bmatrix} \theta \\ \varphi_1 \\ \varphi_2 \\ \dot{\theta} \\ \dot{\varphi}_1 \\ \dot{\varphi}_2 \end{bmatrix} \tag{5.1}$$

where θ is the tool rotation around the vertical axis, and φ_1 and φ_2 are motor and transmission angles respectively.

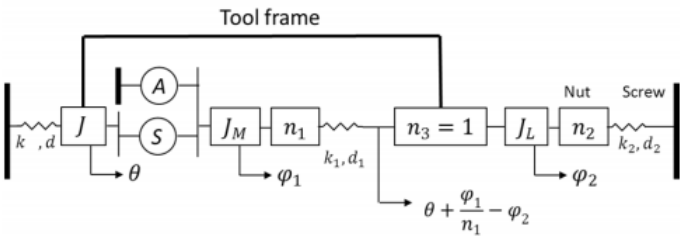

Figure 5.2: Complete model.

The complete system was modelled according to Figure 5.2, which subsequently resulted in the following differential equations. Note that $|T_{L\theta}| = |T_{L\varphi}|$.

$$\begin{aligned} J\ddot{\theta} &= T_{L\theta} - T_o \\ &= k_t\left(\frac{\varphi_1}{n^2} - \varphi_2 + \theta\right) + d_t\left(\frac{\dot{\varphi}_1}{n^2} - \dot{\varphi}_2 + \dot{\theta}\right) - k_o\theta - d_o\dot{\theta} \end{aligned} \tag{5.2}$$

$$\begin{aligned} J_{mg}\ddot{\varphi}_1 &= T_m - \frac{1}{n^2}T_{L\varphi} \\ &= \frac{k_m}{R}u - \frac{k_m k_{emf}}{R}\dot{\varphi}_1 - \frac{k_t}{n^2}\left(\frac{\varphi_1}{n^2} - \varphi_2 + \theta\right) - \frac{d_t}{n^2}\left(\frac{\dot{\varphi}_1}{n^2} - \dot{\varphi}_2 + \dot{\theta}\right) \end{aligned} \tag{5.3}$$

$$\begin{aligned} J_{out}\ddot{\varphi}_2 &= T_{L\varphi} - T_j \\ &= k_t\left(\frac{\varphi_1}{n^2} - \varphi_2 + \theta\right) + d_t\left(\frac{\dot{\varphi}_1}{n^2} - \dot{\varphi}_2 + \dot{\theta}\right) - k_r\varphi_2 - d_j\dot{\varphi}_2 \end{aligned} \tag{5.4}$$

The inertia J is the inertia of the operator and tool calculated according to Equation 5.5.

$$J = m_o \cdot r_o^2 + m_b \cdot r_b^2 + m_t \cdot r_t^2 \tag{5.5}$$

where m and r above are the mass and radius of the operator, the battery, and the tool respectively. The state space model was then updated with the changes.

$$A = \begin{bmatrix} 0 & 0 & 0 & 1 & 0 & 0 \\ 0 & 0 & 0 & 0 & 1 & 0 \\ 0 & 0 & 0 & 0 & 0 & 1 \\ \frac{k_t - k_o}{J} & \frac{k_t}{n^2 J} & -\frac{k_t}{J} & \frac{d_t - d_o}{J} & \frac{d_t}{n^2 J} & -\frac{d_t}{J} \\ -\frac{k_t}{n^2 J_{mg}} & -\frac{k_t}{n^4 J_{mg}} & \frac{k_t}{n^2 J_{mg}} & -\frac{d_t}{n^2 J_{mg}} & -\left(\frac{k_m k_{emf}}{R J_{mg}} + \frac{d_t}{n^4 J_{mg}}\right) & \frac{d_t}{n^2 J_{mg}} \\ \frac{k_t}{J_{out}} & \frac{k_t}{n^2 J_{out}} & -\frac{k_t + k_r}{J_{out}} & \frac{d_t}{J_{out}} & \frac{d_t}{n^2 J_{out}} & -\frac{d_t + d_j}{J_{out}} \end{bmatrix} \tag{5.6}$$

$$B = \begin{bmatrix} 0 \\ 0 \\ 0 \\ 0 \\ \frac{k_m}{J_{mg} R} \\ 0 \end{bmatrix} \qquad C = \begin{bmatrix} 1 & 0 & 0 & 0 & 0 & 0 \\ 0 & 1 & 0 & 0 & 0 & 0 \\ 0 & 0 & 1 & 0 & 0 & 0 \\ 0 & 0 & 0 & 1 & 0 & 0 \\ 0 & 0 & 0 & 0 & 1 & 0 \\ 0 & 0 & 0 & 0 & 0 & 1 \end{bmatrix} \qquad D = \begin{bmatrix} 0 \\ 0 \\ 0 \\ 0 \\ 0 \\ 0 \end{bmatrix}$$

The same controller used in the Coulomb friction model was applied in this model, and the angular motion amplitude of the tool was analyzed as seen in Figure 5.3. The figure clearly shows that the discomfort of the operator is minimal. The deflection angle in transmission was 0.0079 rad, which is slightly smaller than the angle in the bolt tightening model.

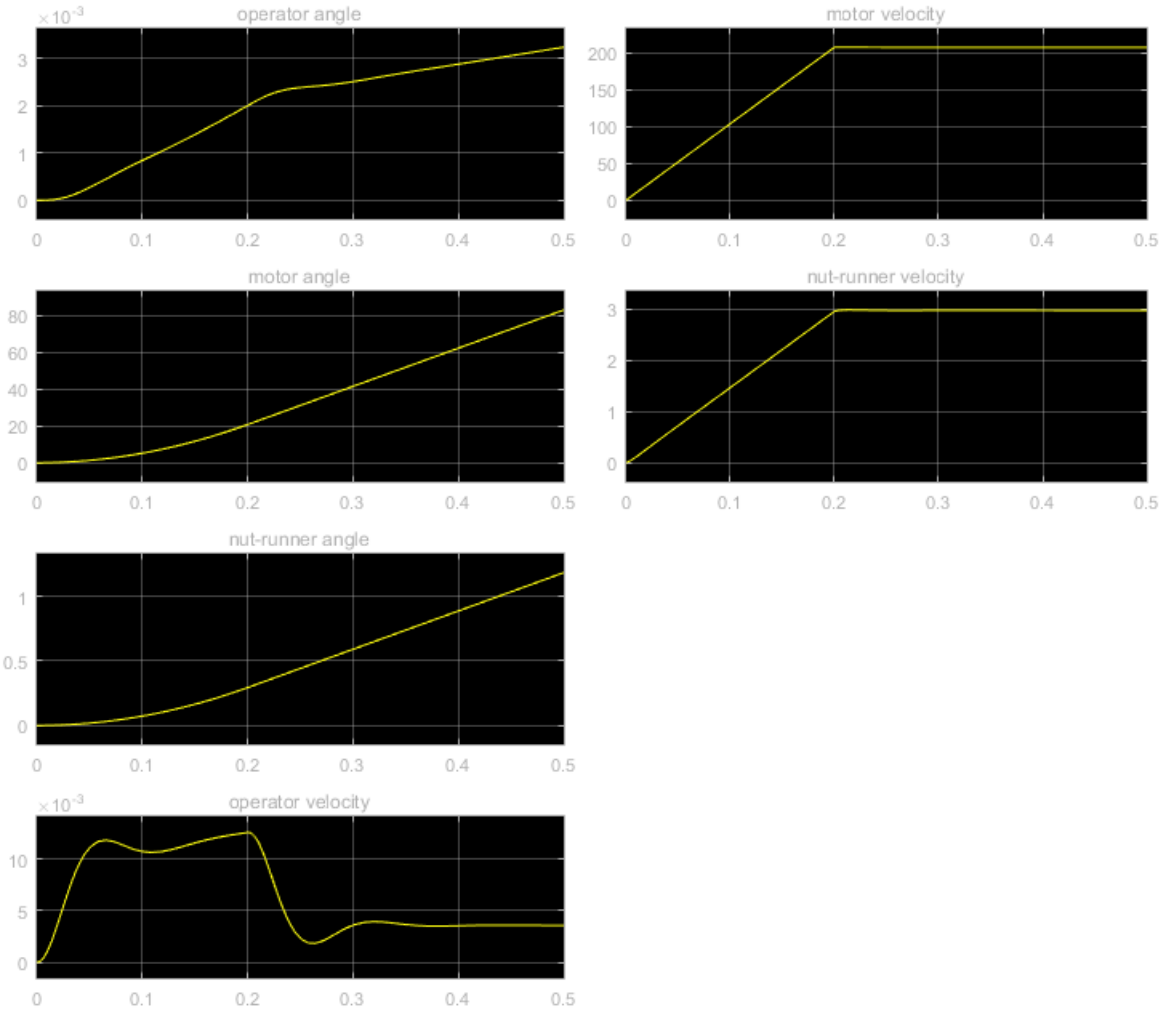

Figure 5.3: System response.

5.1. Energy Consumed

The electrical energy consumed, $E_{electric}$ was calculated by using the following relations

$$\begin{aligned} i &= \frac{U}{R} - \frac{K_m \varphi_1}{R} \\ P &= Ui \end{aligned} \tag{5.7}$$

By implementing said relations in the block diagrams, the energy consumption becomes 45 J for the run-down phase and 41.4 J for the clamping phase. Thus, the total electrical energy

consumed is $E_{electrical}$= 86.4 J.

It is given that the battery can hold 2.6 Ah at 30 V. The energy capacity of the battery can be calculated as

$$E_{store} = 30 \cdot 2.6 \cdot 3600 J = 280800 J \tag{5.8}$$

Therefore, the battery lasts for

$$N = \frac{280800}{86.4} = 3250 \text{rundowns} \tag{5.9}$$

A. Data Sheet of DC-motor

3268 ... BX4 + Encoders

		3268 G		024 BX4	
1	Nominal voltage	U_N		24	Volt
2	Terminal resistance, phase-phase	R		1,45	Ω
3	Output power [1]	$P_{2\ max.}$		32,7	W
4	Efficiency	$\eta_{max.}$		79,5	%
5	No-load speed	n_o		5 500	rpm
6	No-load current	I_o		0,215	A
7	Stall torque	M_H		718	mNm
8	Friction torque, static	C_o		1,7	mNm
9	Friction torque, dynamic	C_v		$1{,}3 \cdot 10^{-3}$	mNm/rpm
10	Speed constant	k_n		220	rpm/V
11	Back-EMF constant	k_E		4,555	mV/rpm
12	Torque constant	k_M		43,5	mNm/A
13	Current constant	k_I		0,0230	A/mNm
14	Slope of n-M curve	$\Delta n/\Delta M$		7,3	rpm/mNm
15	Terminal inductance, phase-phase	L		110	µH
16	Mechanical time constant	τ_m		4,6	ms
17	Rotor inertia	J		60	gcm²
18	Angular acceleration	$\alpha_{max.}$		120	$\cdot 10^3$rad/s²
19	Thermal resistance	$R_{th\,1}$ / $R_{th\,2}$	1,9 / 9,6		K/W
20	Thermal time constant	τ_{w1} / τ_{w2}	17 / 1 060		s
21	Operating temperature range		– 40 ... + 100		°C
22	Shaft bearings		ball bearings, preloaded		
23	Shaft load max.:				
	– radial at 3 000 rpm (4,5 mm from mounting flange)		50		N
	– axial at 3 000 rpm		5		N
	– axial at standstill		50		N
24	Shaft play:				
	– radial	≤	0,015		mm
	– axial	=	0		mm
25	Housing material		stainless steel		
26	Weight		307		g
27	Direction of rotation		electronically reversible		
28	Number of pole pairs		2		
Recommended values - mathematically independent of each other					
29	Speed up to	$n_{e\ max.}$		11 000	rpm
30	Torque up to [1] [2]	$M_{e\ max.}$		47 / 92	mNm
31	Current up to [1] [2]	$I_{e\ max.}$		1,41 / 2,59	A

[1] at 5 000 rpm
[2] thermal resistance $R_{th\,2}$ not reduced / thermal resistance $R_{th\,2}$ by 55% reduced

B. Thorough Derivation of Diameter

The diameter was calculated using the mean value of the basic pitch diameter, d_2, and the minor diameter d_3

$$d_s = \frac{d_2 + d_3}{2} \tag{B.1}$$

The different diameters are defined as

$$d_2 = D - 0.75H \tag{B.2}$$

$$d_3 = d_1 - \frac{H}{6} \tag{B.3}$$

where D is the nominal diameter, H is the height of the triangle on which the thread is based on (see Figure B.1) and d_1 is the basic minor diameter. It is defined as

$$d_1 = D - 1.25H \tag{B.4}$$

Equations B.2-B.4 eventually give us the mean value

$$d_s = D - \frac{13}{12} \cdot H \tag{B.5}$$

where

$$H = \frac{\sqrt{3}}{2} \cdot p \tag{B.6}$$

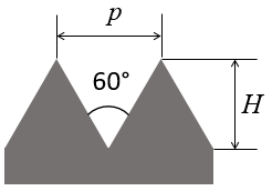

Figure B.1: The pitch and the height of the thread